JOURNAL OF GEOPHYSICAL RESEARCH, VOL. 102, NO. E4, PAGES 9039-9050, APRIL 25, 1997

Absorption and scattering properties of the Martian dust in the solar wavelengths

Maureen E. Ockert-Bell and James F. Bell III
Center for Radiophysics and Space Research, Cornell University, Ithaca, New York

James B. Pollack[1] and Christopher P. McKay
Space Sciences Division, NASA Ames Research Center, Moffett Field, California

François Forget
Laboratoire de Meteorologie Dynamique du Centre National de la Recherche Scientifique, Paris, France

Abstract. A new wavelength-dependent model of the single-scattering properties of the Martian dust is presented. The model encompasses the solar wavelengths (0.3 to 4.3 µm at 0.02 µm resolution) and does not assume a particular mineralogical composition of the particles. We use the particle size distribution, shape, and single-scattering properties at Viking Lander wavelengths presented by *Pollack et al.* [1995]. We expand the wavelength range of the aerosol model by assuming that the atmospheric dust complex index of refraction is the same as that of dust particles in the bright surface geologic units. The new wavelength-dependent model is compared to observations taken by the Viking Orbiter Infrared Thermal Mapper solar channel instrument during two dust storms. The model accurately matches afternoon observations and some morning observations. Some of the early morning observations are much brighter than the model results. The increased reflectance can be ascribed to the formation of a water ice shell around the dust particles, thus creating the water ice clouds which *Colburn et al.* [1989], among others, have predicted.

1. Introduction

The atmospheric dust of Mars is a key radiative factor in the heating of the atmosphere and plays an important role in radiative and dynamical models of the Martian atmosphere. The properties that determine the radiative effects of the dust and that are necessary for modeling studies are the particle size distribution, shape, and complex index of refraction [*Pollack et al.*, 1995].

The basic approach in previous work has been to assume that the optical indices are described by a known terrestrial material or soil type. A variety of materials have been examined including basalt and basaltic glass as well as a variety of weathering products like limonite, montmorillonite, and palagonite [*Toon et al.*, 1977; *Clark et al.*, 1990; *Drossart et al.*, 1991; *Kahn et al.*, 1992; *Clancy et al.*, 1995]. All of these materials represent classes of compounds and not a unique mineralogy. Therefore, the optical indices are averages, defined as representative of these materials.

Various particle size distributions have been suggested using these assumed mineralogies. *Toon et al.* [1977] employ the optical properties of montmorillonite and a modified-gamma particle size distribution to determine the mean infrared properties of the dust from Mariner 9 Infrared Imaging Spectrometer (IRIS) data. Their best fit size distribution for α=2 and γ=0.5 is a mode radius of 0.4 µm. Using these values, it is possible to calculate the first two moments of the size distribution: r_{eff} = 2.70 µm and ν_{eff} = 0.38 µm. *Drossart et al.* [1991] use the optical properties of basalt to extract the size distribution from Phobos-2 Imaging Spectrometer (ISM) data. For a modified-gamma size distribution (with α=2 and γ varied) they find that r_{eff} = 1.24 µm for ν_{eff} = 0.25 µm was the best fit to the data in the upper atmosphere. *Clancy et al.* [1995] assume a "palagonitelike" composition for their analysis of the Mariner 9 IRIS and Viking Infrared Thermal Mapper (IRTM) Emission Phase Function (EPF) data. They define a best particle size distribution (r_{eff} = 1.8 µm for ν_{eff} = 0.8 µm) based on the fit of the 20- to 30-µm dust opacity and the visible to 9-µm dust opacity ratio found by *Martin* [1986].

An alternative approach to determining the properties of the Martian atmospheric dust is to begin with observations of the reflected and emitted light from Mars and to fit the complex index of refraction and particle size distribution and shape to these observations, with no assumed mineralogy. This approach was employed by *Pollack et al.* [1995] (hereafter referred to as paper 1). Viking Lander images were used to define a best fit particle size distribution, shape, and single-scattering albedo for several solar wavelengths. Their best fit size distribution (r_{eff} = 1.85 µm for ν_{eff} = 0.51 µm) is not greatly different from the sizes found by *Drossart et al.* [1991] and *Clancy et al.* [1995]. The calculated single-scattering properties of the aerosols (Table 1) are not greatly different

[1]Deceased, June 13, 1994

Paper number 96JE03991.
0148-0227/97/96JE-03991$09 00

Table 1. Single-Scattering Properties of the Martian Dust Particles at Viking Lander Wavelengths

λ_{eff}	ω_0	g	Q_{ext}	n_i
0.49	0.79	0.68	2.82	0.0100
0.55	0.84	0.66	2.89	0.0070
0.66	0.94	0.63	3.04	0.0025
0.86	0.89	0.65	3.11	0.0065

Data are from *Pollack et al.* [1995].

from the results of *Pollack et al.* [1979] and do have basaltic features, as expected. Although not much was learned about the actual mineralogy of the dust, it appears that the light-scattering properties of the dust can be accurately modeled with this approach.

In this paper, we begin with the analysis of the Viking Lander images in paper 1 to provide the particle size distribution, shape, and single-scattering properties at four wavelengths in the visible (0.5 - 0.86 μm). Although the wavelength coverage is limited, observations at several phase angles provide an accurate determination of the single-scattering properties. We are able to extend these results to include the solar spectrum (0.3 - 4.3 μm) by incorporating observations made by ground-based observers and the Phobos-2 spacecraft into our analysis. The new model of single-scattering properties is then used as a basis for models of Viking Orbiter IRTM solar channel observations taken during the 1977 dust storms. We find that the new model (marsdust) can predict the observed solar reflectance at a variety of phase angles to within 10%. We find that there is a discrepancy between the accuracy of modeled reflectances for morning and afternoon observations. We discuss four hypotheses for the inferior model results of morning observations and conclude that the most likely theory attributes the model inaccuracy to the formation of water ice clouds in the morning, which would greatly increase the brightness of morning observations.

2. Data and Methods

The relative lack of remotely sensed observations of dust storm periods creates difficulties when attempting to define a wavelength dependent model of the atmospheric dust. Although there are some Viking Lander and Orbiter data during dust storm periods, the wavelength coverage is not adequate. Fortunately, more recent observations with more extensive wavelength coverage exist, albeit without dust storm conditions and with poorer phase angle coverage. However, the optical properties of the dust are probably related to the optical properties of the surface. If one were to assume that the bright surface areas were actually composed of an optically thick layer of dust and that this dust is the source of the atmospheric dust, then it is possible to use observations obtained of bright surface areas at solar wavelengths to infer the single-scattering properties of the atmospheric dust.

2.1. Dust Properties in the Solar Wavelengths

Since we utilize the results from paper 1, we briefly review their work. Images taken by the Viking Lander 1 and 2 cameras with the blue, green, red, IR1 and survey filters were analyzed. The observed reflectances at a variety of phase angles (from 10 to 150 degrees phase) are modeled using the doubling/adding radiative transfer method. This method includes a Hapke representation for the surface [*Hapke,* 1981, 1986] and nonspherical particle theory for the atmospheric scatterers [*Pollack and Cuzzi,* 1980]. The atmosphere is modeled using the doubling method and the surface is added to the atmosphere system using the adding method [*Hansen,* 1969]. The resulting reflectance is computed as *I/F* (or radiance factor as defined by *Hapke* [1986]). An iterative approach is used to find the best fit values for the particle size, shape, and single-scattering properties.

Paper 1 uses a lognormal size distribution with nonspherical particles to describe the Martian aerosols. The best fit values for the first two moments of the phase function are effective radius r_{eff} = 1.85 μm and effective width v_{eff} = 0.51 μm. The corresponding single-scattering properties (Table 1) are found to be more absorbing than previously modeled montmorillonite samples and less absorbing than basalt samples. The single-scattering albedo is not unreasonable as compared to these materials, with the exception of 0.86 μm. If one assumes that the spectrum of the atmospheric dust is directly comparable to that of the surface, then the albedo at 0.86 μm would be greater than or equal to the other wavelengths (e.g., see Figure 1). Paper 1 points out that the IR1 diode had a large blue leak, which may greatly effect the value given here. The aerosol model presented in paper 1 provides the necessary information for the next step, to expand the wavelength range to encompass the solar spectrum.

2.2. Observations of Bright Surface Regions

Owing to the lack of well-calibrated dust storm reflectance spectra at solar wavelengths, we need to find an alternate source of data. There is a large inventory of remotely sensed

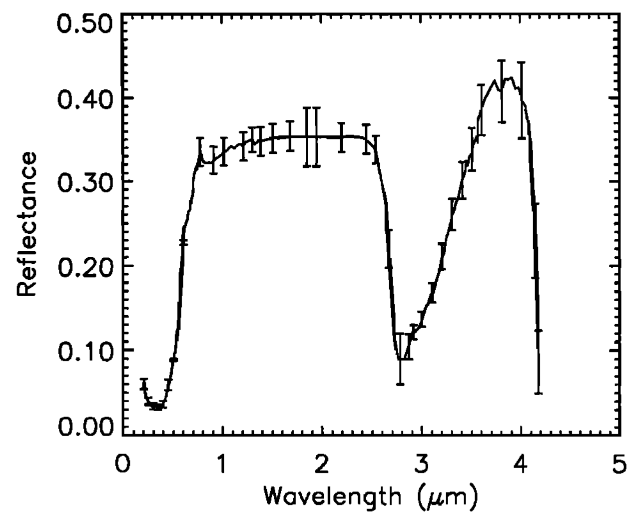

Figure 1. Composite spectrum of the Amazonis region. Wavelength range 0.204-0.365 μm: OAO/WEP Mars whole-disk UV spectrum from *Owen and Sagan* [1972] scaled by 0.84 to match 0.396-0.774 μm data. Wavelength range 0.396-0.774 μm: telescopic data from *Bell et al.* [1990], scaled to match reflectance of *Mustard and Bell* [1994] ISM near IR data. Wavelength range 0.774-2.898 μm: Phobos-2 ISM data from *Mustard and Bell* [1994]. Wavelength range 2.898-4.181 μm: telescopic IRTF data from *Roush et al.* [1992] with 275 K thermal component removed, scaled by 1.20 to match ISM data.

Mars data at times when the atmosphere was quiescent. It is possible to equate surface data with atmospheric dust data, thus improving our "dust" database. The theory that the bright surface regions are a source of atmospheric dust was advocated by *McCord et al.* [1977], who noted that the visible and near-IR spectra of optically thick dust as seen in spectra taken at Mauna Kea in 1973 are similar to that of bright surface regions. Therefore, we assume that the bright surface areas are spectrally the same as the atmospheric dust. Data taken of bright surface areas during times of very low dust loading would be adequate then to estimate the optical properties of the atmospheric dust.

The 1988 Earth-Mars opposition fit this criterion. The dust loading was unusually low ($\tau \approx 0.1$). It was also close in time to the Phobos-2 spacecraft mission, which orbited Mars during late 1988 and early 1989. *Drossart et al.* [1991] found low dust optical depths ($\tau \approx 0.2$) during the mission as well. A comparison of ground-based data and Phobos data taken during this time period found that the spectra for various regions concurred [*Mustard and Bell,* 1994]. Several spectra of the bright regions fit the low dust loading criterion for this research.

Mustard and Bell [1994] produced a set of composite Mars bright and dark region spectra by using 0.4- to 1.0-μm ground-based telescopic data taken from Mauna Kea Observatory [*Bell et al.,* 1990] and scaling and merging them with well-calibrated 0.76 to 3.14 μm reflectance spectra of the same regions observed close in time and from Martian orbit by the Phobos-2 ISM instrument [*Bibring et al.,* 1989; *Mustard et al.,* 1993].

In order to encompass all of the solar wavelengths, these composite spectra were extended to 0.2 to 4.2 μm. This was achieved by first scaling the Mars whole-disk UV observations obtained by the Orbiting Astronomical Observatory/Wisconsin Experiment Package (OAO/WEP) [*Wallace et al.,* 1972; *Owen and Sagan,* 1972] to match the short-wavelength end of the *Mustard and Bell* [1994] composite spectra.

We used the L band ground-based Infrared Telescope Facility (IRTF) radiance factor spectrum of spot 86-4 from *Roush et al.* [1992] to produce the longer wavelength segments of the extended spectra. Before scaling and merging the *Roush et al.* [1992] 2.90- to 4.18- μm spectrum, though, we removed an estimate of the Mars thermal emission component included in the spectrum. This was achieved by first using the observational and photometric parameters for the spectrum and the NASA/Ames Mars general circulation model (J. Schaeffer, personal communication, 1994) to estimate the temperature (275 K) of the region of the surface corresponding to spot 86-4, and then using the technique of *Houck et al.* [1973] to estimate and subtract the Planck thermal contribution from the observed radiance. The thermal contribution varied from negligible below 3.2 μm to 50% of the radiance at 4.2 μm. The values of the thermally corrected *I/F* spectra are extremely sensitive to the assumed surface temperature because of the exponential nature of the Planck function. This is especially true at the longest wavelengths. For example, an increase of 5 K in the modeled surface temperature leads to a 25% decrease in the corrected *I/F* at 4.2 μm.

The result of these steps is a set of composite 0.20- to 4.18-μm reflectance spectra of Martian surface regions composed of 0.20- to 0.37- μm OAO/WEP data, 0.40- to 0.77-μm ground-based telescopic data, 0.77- to 2.90-μm Phobos-2 ISM data, and 2.90- to 4.18-μm ground-based telescopic data, all calibrated to reflectance based on the ISM data calibration. This expanded composite data set includes observations of two bright surface areas: Amazonis and Tharsis. The Amazonis and Tharsis spectra were so close in value that we simply chose Amazonis as the representative bright region spectrum. The final step was to interpolate over the major Mars atmospheric H_2O and CO_2 absorptions at 1.44, 2.0, and 2.7 μm in order to produce an estimate of the "dust only" spectrum without any atmospheric spectral contribution. Thus our bright surface representation is defined by the spectrum shown in Figure 1 for the solar wavelengths (0.4 to 4.2 μm).

2.3. Modeling the Dust Using Bright Surface Observations

The atmospheric dust optical properties have been defined for a limited number of wavelengths using the Viking Lander data. A spectrum of a bright surface region has been manipulated to give a representation of the light-scattering behavior of the surface over all solar wavelengths. The next step is to extract dust properties at all wavelengths from the bright surface spectrum.

In order to relate the surface dust to airborne dust, we must make certain assumptions. It is important to define which properties are the same for the two species. The complex index of refraction is an intrinsic property of the particles, regardless of whether they are in the atmosphere or on the surface, closely spaced or not [*van de Hulst,* 1981]. We can use this relationship to define the surface dust single-scattering albedo and use Hapke theory to relate the surface albedo to the complex index of refraction. In order to do this we need to have a priori information of the dust refractive index, which we take from the analysis of paper 1. Since the effective particle size distribution, or grain size, and the separation of particles does vary between the atmospheric aerosols and the surface dust, we treat the two species differently by using nonspherical particle theory to descibe the scattering properties of the aerosols and Hapke theory to describe the scattering properties of the surface particles.

Hapke's theories of bidirectional reflectance spectroscopy were used extensively in this analysis [*Hapke,* 1981, 1986]. There are a number of parameters that are important to Hapke theory. The parameters used in this analysis were the single-scattering albedo ω_0, the width of the opposition effect h, and the magnitude of the opposition effect $S(0)$. The phase function of the particles was assumed to be a single-lobed Henyey-Greenstein (asymmetry factor g). Hapke's roughness parameter θ was found to effect the results less than 1% and was not fit in order to reduce the number of parameters in this investigation.

A quadratic was fit to each of the Hapke parameters PH_i such that

$$PH_i = a_i + b_i\,(I/F_\lambda) + c_i(I/F_\lambda)^2 \tag{1}$$

The initial value of each I/F_λ was defined for the geometry of each surface observation and modeled using the values of the Hapke parameters for the Viking Lander 1 (VL1) site given by *Arvidson et al.* [1989]. The values of each Hapke parameter were defined at all wavelengths by calculating the polynomials using the observed data. Each Hapke parameter was examined at all wavelengths to be sure that the results remained "physical." That is, the single-scattering albedo and B(0), the backscatter function that describes the opposition effect, had to have values between 0 and 1, and the width of the opposition effect had to remain close to the values given in *Arvidson et al.* [1989].

From equation (1), we have obtained a first estimate of the single-scattering albedo ω_o at each wavelength of interest. In the next step, we held constant the other three Hapke parameters and used a Newton iteration scheme and the Taylor expansion theorem to increment ω_o so that the theoretical *I/F* matched the observed *I/F*. That is, for the *j*th iteration, let I/F^t_j be the theoretical Hapke value found from using the latest estimate of ω_o, ω_{oj}, and I/F^{obs}. Then the value for the next iteration (j+1) is found from

$$I/F^{obs} = I/F^t_j + \frac{\delta I/F^t_j}{\delta \omega_o} \Delta\omega_{o(j+1)} \tag{2a}$$

$$\frac{\delta I/F^t_j}{\delta \omega_o} = \frac{(I/F^t_+ - 2\,\omega_{oj}\,\varepsilon\, I/F^t_-)}{\Delta\omega_{o(j+1)}} \tag{2b}$$

where I/F^t_+ and I/F^t_- are the theoretical values of *I/F* calculated using ω_{oj} +/- $\varepsilon=10^{-3}$. Iterations were performed until the value of ω_{oj} agreed with the previous value to within ε. For most of the wavelengths, only two or three iterations were necessary for convergence to occur. At the extreme shortward and longward ends, several iterations were necessary, resulting in a change of a few percent in the value of ω_o.

Once the single-scattering albedo for the bright surface was found, it was possible to relate ω_o to the imaginary index of refraction, again using Hapke theory (see *Hapke* [1981], section 3: Single Particle Scattering). We considered the situation described by Hapke in which the surface consists of large, closely spaced particles of one type ($\omega_o = Q_s$) and in which the internal scattering s is neglected (i.e., $s = 0$). In this case, ω_o is given by

$$\omega_o = Q_s = S_E + \frac{(1-S_E)\,(1-S_I)\,\exp(-x)}{1 - S_I\,\exp(-x)} \tag{3a}$$

and

$$x = \frac{2}{3}\,\alpha D = \frac{8\,\pi\, n_i D}{3\,\lambda} \tag{3b}$$

where D is the grain size, S_E is the angularly averaged reflection coefficient for light externally incident on a grain, and S_I is the corresponding reflection coefficient for light incident from the inside of the particle. To find S_E and S_I we assumed that the real index of refraction did not vary with wavelength and that the imaginary index was much smaller than the real: valid assumptions for most of the wavelengths analyzed when compared to basalts (see Figure 2). The values for the Amazonis spectrum were approximately $S_E = 0.153$ and $S_I = 0.596$.

By manipulating equations (3a) and (3b), we can find n_i of the Martian dust at all wavelengths by using the calculated bright surface albedo at all wavelengths and the calculated values of S_E and S_I. First, we find the effective grain size, D, by using the values of n_i from paper 1 and ω_o from the surface analysis.

$$D = \frac{3\,\lambda}{8\,\pi\, n_i}\left(-\ln\left(\frac{\omega_o - S_E}{(1-S_E)(1-S_I)+(\omega_o S_I - S_E S_I)}\right)\right) \tag{4}$$

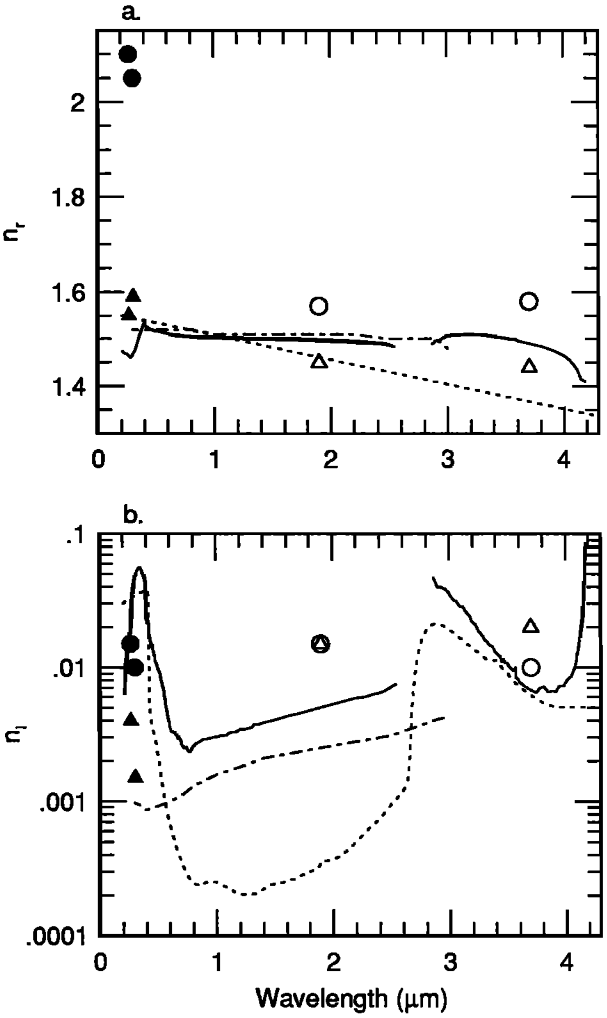

Figure 2. Comparison of the real and imaginary parts of the complex index of refraction of the marsdust model (solid line) and candidate materials: a palagonite from *Clark et al.* [1990] (dotted line), basalt from *Pollack et al.* [1973] (dashed line), basalt from *Egan et al.* [1978] (open circles), montmorillonite 219b from *Toon et al.* [1977] (open triangles), Mariner 9 UVS model results from *Pang et al.* [1976] (solid circles), and from *Chylek and Grams* [1978] (solid triangles).

Initially, we used the value for the green filter, since that filter had the fewest leaks from other wavelengths. We then solved for n_i at all wavelengths using the inverse of equation (4) and the surface albedos. We checked the values of n_i by comparing the values at the Viking image wavelengths to the new n_i (Figure 2b). In all cases except at 0.86 µm, the calculated values were within a percent of the Viking values. As noted earlier, this wavelength was suspect in the analysis of paper 1.

In the wavelength region close to 0.3 µm and above 3.5 µm, the assumption that $n_i \ll n_r$ was not valid. Since reasonable results were found on either side of 0.3 µm, a polynomial was fit to the calculated values of n_i and the approximation was spliced between 0.3 and 0.4 µm. The values of n_i in this wavelength region have a relatively high associated error of 20-40%. The values of n_i above 3.5 µm are as calculated with the above method but with an associated error of 25%. Even though the error associated with the values of n_i in these wavelength regions is large, the error of n_r and

Table 2. Single-Scattering Properties of the Martian Dust Particles at Solar Wavelengths

λ	ω_0	g	Q_{ext}	n_r	n_i
0.21	0.72	0.81	2.60	1.47	0.008
0.30	0.61	0.88	2.58	1.48	0.038
0.35	0.61	0.86	2.61	1.50	0.039
0.40	0.63	0.84	2.65	1.51	0.034
0.50	0.78	0.73	2.82	1.52	0.011
0.60	0.91	0.67	2.98	1.51	0.004
0.67	0 93	0.65	3.04	1.51	0.003
0.70	0.94	0.65	3.06	1.51	0.003
0.80	0.95	0.64	3.13	1.50	0.003
1.015	0.95	0.63	3.24	1.50	0.003
1.21	0.95	0.63	3.32	1.50	0.004
1.39	0.96	0.63	3.36	1.50	0.004
2.20	0.95	0.63	3.25	1.49	0.006
2.49	0.95	0.63	3.11	1.49	0.007
2.90	0.80	0.67	2.77	1.50	0.045
3.00	0.81	0.67	2.77	1.51	0.039
3.19	0.88	0.65	2.76	1.52	0.022
3.40	0.93	0.64	2.69	1.52	0.013
3.60	0.95	0.63	2.59	1.51	0.009
3.78	0.96	0.63	2.49	1.51	0.008
3.98	0.95	0.63	2.36	1.50	0.008
4.15	0.88	0.65	2.23	1.50	0.025

Error of ω_o, g, Q_{ext}, and n_r is 5% for λ<0.4 or λ>3.0 µm, and 2% otherwise.

Error of n_i is 30% for λ<0.4, 25% for λ>3.0 µm, and 15% otherwise

the single-scattering properties is about 5% owing to the very low values of n_i.

A final step was added to determine a more realistic result. We had assumed that the real index of refraction was constant over the solar wavelengths and equal to 1.5, which is a reasonable value for a basalt [e.g., *Pollack et al.*, 1973]. It is more likely that n_r varies a small amount over these wavelengths (given the values of such candidate materials as basalt, montmorillonite, and palagonite). A Kramers-Kronig routine was employed to find the change in the real index given the changes in the imaginary [*Warren*, 1984]. The value of n_r near the center of the wavelength range was set to 1.5, and several iterations were performed to find the best fit (Figure 2a).

We used the new values of the complex index of refraction and nonspherical particle theory to calculate the single-scattering properties of the "atmospheric dust," Q_{ext}, g, and ω_0 (Table 2). The range of values for the new "marsdust" model n_r and n_i is reasonable when compared to the work of other researchers and to candidate basaltic materials, as shown in the following section.

The errors of the values presented in Table 2 were found by modeling the error of the initial surface model; that is, for each observation point, there was an associated error and that propagated through the analysis. Although there were a number of assumptions made throughout the process of calculating the marsdust model, the largest error was in the initial bright surface model and, in particular, the removal of the atmospheric contribution to the brightness. Though the Phobos and Mauna Kea spectra were well understood and had an error of 2% - 8%, the data in the UV and near IR have much larger errors (15% or greater). It was assumed that scaling the ultraviolet data to the values at longer wavelengths removed some of the atmospheric contribution, but a more thorough investigation is needed. Likewise, modeling the thermal contribution to the near-IR wavelengths may not have entirely corrected the atmospheric contribution.

Further problems might arise from the assumptions made in the Hapke modeling. The use of a single-lobed Henyey-Greenstein function for the surface scattering might be questionable since it is notoriously bad at modeling backscattering [e.g. *Domingue et al.*, 1991]. However, we used the surface analysis of *Arvidson et al.* [1989] as our initial model, and it fit the surface scattering at the VL1 site quite well. Our second assumption, that the particles on the surface are large, closely spaced, and of one type may not be accurate, but since we are not modeling the specific mineral composition of the surface our "monomineralic" surface can actually be a combination of minerals. We believe that these errors are small in comparison with the assumptions made in the preparation of the bright surface spectrum.

The assumption that the internal scattering was insignificant (equation (3a)) may be incorrect. Irregularly shaped particles do have internal scattering off of their interior surfaces [*Hapke*, 1981]. However, a direct solution of equation (24) in *Hapke* [1981] for the imaginary index of refraction is not possible. A grid search of possible values of s (ranging from 0 to 5) was performed. Although s can be any number, the chi squared fit to the observed surface albedo was high when $s > 1$. The best fit value of s was 0.4, although only the longest and shortest wavelengths were affected. The imaginary indices below 0.5 µm and above 2.5 µm (Table 2) were adjusted 10 to 30% from the original to account for internal scattering. The real index and other parameters were recalculated as well, given the new imaginary indices. Though a number of assumptions were made to find the various parameters for the marsdust model, the results presented in Table 2 reproduce spacecraft observations well, as is shown in the next section.

3. Discussion

3.1. Findings

We have found the single-scattering properties of the Martian dust for wavelengths encompassing the solar spectrum from 0.2 to 4.3 µm (Figure 2 and Table 2). The process that we used was empirical and by definition matches the Viking Lander results from paper 1. The new real and imaginary indices represent a macroscopic average of the actual particles, and so the actual compositional information is lost. However, they can be compared to laboratory spectra of minerals and compounds, to the work of other researchers, and to observations by other spacecraft to determine their validity.

The complex index of refraction values of a number of minerals and compounds have been applied toward the investigation of the Martian surface and airborne dust. Models currently include mostly basaltic compounds and weathered materials like clays and palagonite. The candidate materials (Figure 2) can be compared to our dust model. It is important to note that the work done by other researchers most often does not include all solar wavelengths; either it is only necessary to find a few wavelengths to match the observations or a wavelength-integrated value is used. Here we examine all wavelengths for several candidate materials.

Montmorillonite 219b is the canonical compound used to represent Martian dust. *Toon et al.* [1977] specifically state that montmorillonite 219b, by itself, does not match the Mariner 9 IRIS data because it is too bright. Additionally, they did not publish values for all wavelengths below 2.5 μm. Here we show values from *Egan et al.* [1978] as well as the values in the near IR from *Toon et al.* [1977]; these are the values used by *Korablev et al.* [1993] in their analysis of Phobos-2 data. Two other compounds, basalt [*Pollack et al.*, 1973] and palagonite [*Clark et al.*, 1990], are used as candidate compounds as well. In all of these cases the values of the real index of refraction for the marsdust model are reasonably close to the values of the other compounds. This is also true for the imaginary index of refraction; the marsdust model values are reasonably close to the other models.

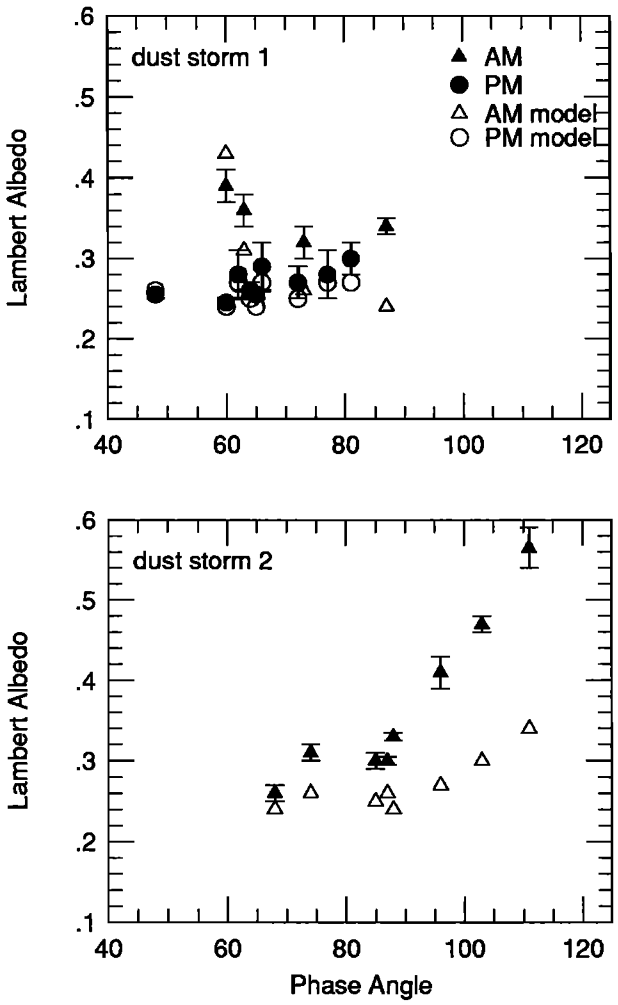

Figure 3. Observations of the Viking Lander 1 site taken by the Viking Orbiter IRTM solar channel during dust storms 1 and 2. The errorbars encompass the range of brightness observed at a particular phase angle over several orbits during each dust storm. The open circles and triangles are the IRTM observations modeled using the marsdust particle size distribution, shape, and single-scattering properties.

The real and imaginary indices in the ultraviolet do not closely match previous investigations. The Mariner 9 UV spectrometer took several measurements at 0.3 and 0.2 μm in 1971. Two research papers analyzed these data. The methods used by the authors are similar to those of our investigation, yet the results differ. *Pang et al.* [1976] assume spherical particles and investigate a wide range of particle size distributions and refractive indices. *Chylek and Grams* [1978] assume nonspherical particle shape and perform similar calculations. Both of these studies find the dust to be less absorbing at 0.2 and 0.3 μm than the marsdust model. This is in direct contrast to the results discussed in *Wolff et al.* [this issue], who found that a "darker" dust in the UV produces acceptable fits to data taken of Hellas and the polar regions by the Hubble Space Telescope (HST) at 0.26, 0.37, and 0.41 μm. The ultraviolet interaction with the dust is indeed "problematic" and needs to be more systematically modeled in order to work out these discrepancies.

3.2. Validation of the Model

We can test the limitations of the marsdust model by using a data set not used in the analysis, the Viking Orbiter IRTM solar channel data. The solar channel observations were taken in seven channels with a broad spectral bandwidth (0.3 - 3.0 μm) (see *Kieffer et al.* [1977] and *Chase et al.* [1978] for instrument details). The data that we used were calibrated and converted into Lambert albedos A_L, which is the radiance factor *I/F* [*Hapke* 1981] divided by the cosine of the incidence angle.

The data we selected are from the Viking Lander 1 site taken during the peak of the two dust storms (Figure 3). The observations are separated into dust storm 1 and 2 and by time of day, where morning is "AM" (0-4 hours after sunrise) and afternoon is "PM" (greater than 4 hours after sunrise). There are not enough data taken of the Viking Lander 2 site to be useful for this comparison. We concentrate on the VL1 site because it is possible to obtain concurrent optical depth measurements from the VL1 solardiode (Table 3). For this comparison, a dust storm is defined as the time at which the dust optical depth was high enough that the surface properties contributed little to the overall brightness (for dust optical depths greater than 1, the surface contribution is less than 1% of the total top-of-atmosphere reflected brightness).

The IRTM data were modeled using our best particle model (n_r and n_i from Figure 2 and particle size distribution and shape from paper 1). Fifteen wavelengths were chosen to represent the absorption and scattering patterns of the particles (Table 2), and a bright surface model defined in Hapke parameters was used to represent the surface properties around the VL1 site. The specific observing geometry and dust optical depth of each IRTM observation was modeled (Table 3).

The model output was weighted by the product of the solar spectrum S_λ [*Allen*, 1985] and the instrument response function R_λ [*Chase et al.*, 1978] to give a simulated IRTM brightness:

$$I/F_{\text{model IRTM}} = \frac{\int_{0.3}^{3.0} I/F_\lambda \, S_\lambda \, R_\lambda \, d\lambda}{\int_{0.3}^{3.0} S_\lambda \, R_\lambda \, d\lambda} \quad (5)$$

Table 3. Viking Orbiter IRTM Observations Taken of the Viking Lander 1 Site

incidence angle, deg.	emission angle, deg.	phase angle, deg.	τ	A_L	L_s	TAS
				Dust Storm 1		
67	26	87	0.9	0.34 ± 0.01	207 AM	1.7 - 2.1
65	36	73	0.9	0.32 ± 0.02	207 AM	1.7 - 2.1
65	54	63	0.9	0.36 ± 0.02	207 AM	1.7 - 2.1
64	69	60	0.9	0.39 ± 0.02	207 AM	1.7 - 2.1
40	38	64	1.1	0.26 ± 0.01	207 PM	6.7 - 8
42	20	60	1.1	0.245 ± 0.005	207 PM	6.7 - 8
41	29	65	1.1	0.255 ± 0.005	207 PM	6.7 - 8
44	42	72	1.1	0.27 ± 0.02	207 PM	6.7 - 8
45	52	77	1.1	0.28 ± 0.03	207 PM	6.7 - 8
46	58	81	1.1	0.30 ± 0.02	207 PM	6.7 - 8
40	27	66	2.3	0.29 ± 0.03	215 PM	6 - 7
38	27	62	2.3	0.28 ± 0.03	215 PM	6 - 7
36	32	48	2.3	0.255 ± 0.005	215 PM	6 - 7
				Dust Storm 2		
70	26	85	1.1	0.30 ± 0.01	268 AM	1.5-1.7
52	41	87	1.2	0.30 ± 0.005	269 AM	4
65	9	68	1.2	0.26 ± 0.01	269 AM	3
74	56	111	2.5	0.565 ± 0.025	278 AM	1.3
74	43	103	2.5	0.47 ± 0.01	278 AM	1.4
73	33	96	2.5	0.41 ± 0.02	278 AM	1.5
69	6	74	2.5	0.31 ± 0.01	278 AM	1.9
82	13	88	2.7*	0.33 ± 0.005	282 AM	0.7

A_L is the Lambert albedo; L_s is the aerocentric longitude of Mars; TAS is the time after sunrise, in hours.
* Lower bound.

The simulated brightness was then divided by the cosine of the incidence angle to give a model Lambert albedo.

The model simulations of solar channel data are remarkably well matched to the observations (Figure 3). For the PM observations, the model results are within 10%. The models of the morning observations are not as good, differing by as much as 40%.

The observations made by the IRTM solar channel over the VL1 site during the two dust storms provide an interesting data set. It would have been a much more comprehensive data set had more afternoon data been taken. Nonetheless, the data set provides us with the ability to discern the conditions for which this dust model are valid. The discrepancies between the seemingly accurate model for afternoon data and inaccurate model for morning data can be explained with four hypotheses:

1. The morning observations may be brighter due to observation geometry or error in observation pointing rather than the particle properties.

2. The AM particle size may be different from our value of 1.85 μm. A reasonable assumption would be that the particles are smaller, as suggested by Drossart *et al.* [1991], since particle sedimentation would cause smaller particles to be seen from above, as with the IRTM data, as opposed to viewed from the surface, as with the VL data. It is also reasonable to assume that the particles might be larger than our value. In the first dust storm the morning data were taken early in the storm (L_s 207), and vigorous mixing from the dust storm may have brought larger particles to the upper atmosphere.

3. The AM particles may be less absorbing than predicted by this model. Several investigators have proposed brighter particles such as montmorillonite and palagonite.

4. The morning data may be affected by the presence of ice clouds, which may form during the night or early morning hours. In this case, the darker dust particles would be covered by a bright ice shell, which would increase the overall brightness.

These four hypotheses have been investigated using our radiative transfer model and assuming the dust composition presented in this research and by other researchers.

3.2.1. Observation geometry of IRTM data. It is possible that the early morning IRTM observations are taken at a phase angle that our marsdust model does not recreate well. In the analysis of the VL1 site data set (Table 3) the afternoon observations are taken at phase angles between 45° and 80°. Although several of the morning observations are taken at similar phase angles, several are also at angles greater than 80°. In order to determine the extent of dependence of the marsdust model results on the observation

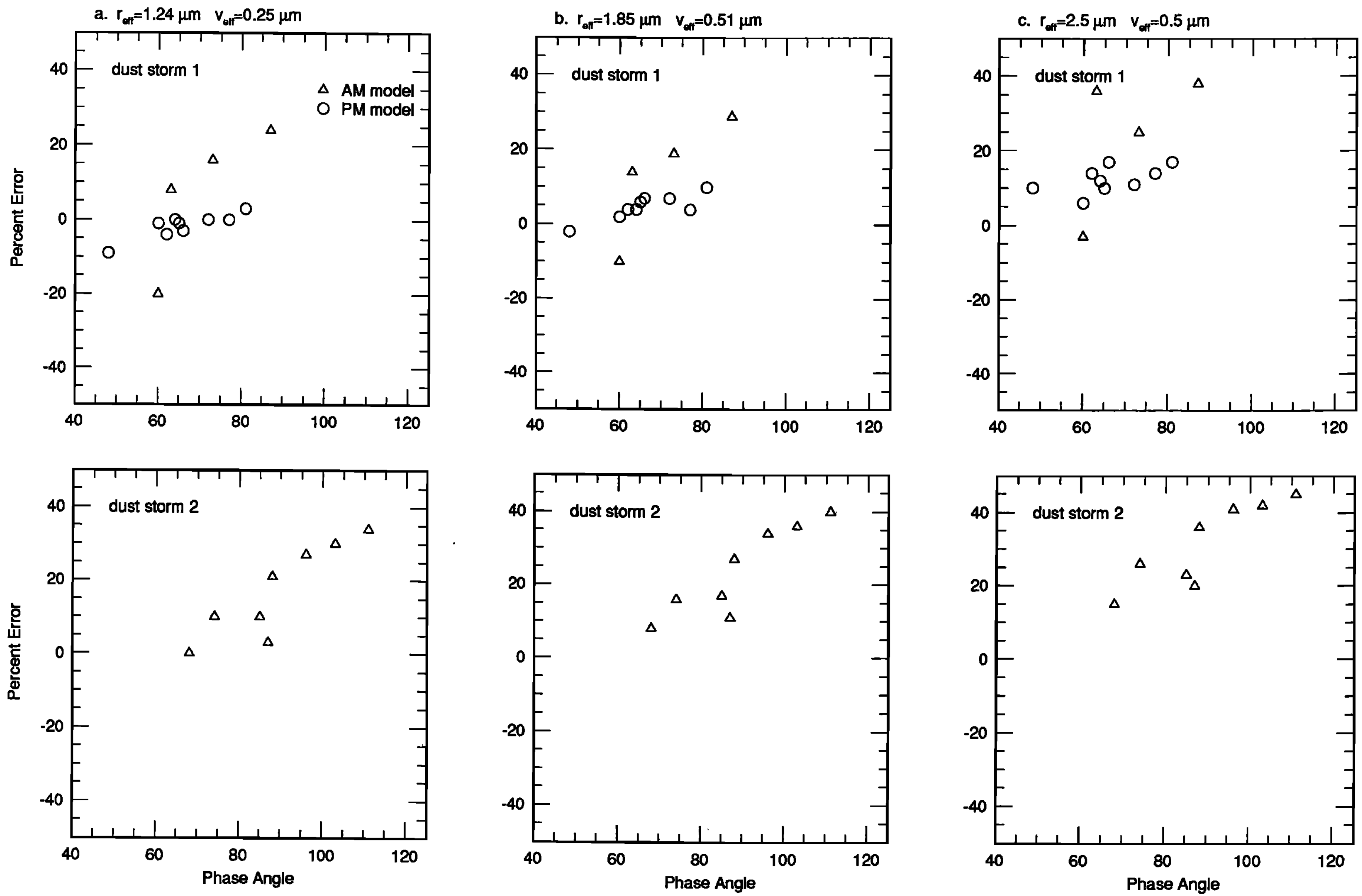

Figure 4. Comparison of the error in model results for three particle size distributions with the complex index of refraction of the marsdust model. (a) The smallest particle size as given in *Drossart et al.* [1991]. (b) The intermediate size as given by *Pollack et al.* [1995]. (c) The largest particle size as given by *Toon et al.* [1977].

geometry, we analyzed all northern hemisphere data that were taken by the IRTM solar channel during the peak of the dust storms. There was such a large amount of data that the observations were binned by latitude, longitude, and time of day. We analyzed the data that were within 2-sigma of the mean reflectance (that is, $A_L = 0.33 \pm 0.08$).

There were a total of 1676 observations that fulfilled this requirement. We simplified the modeling process for these observations by using the wavelength-integrated values for the refractive indices (λ_{eff}=0.88 μm, n_r= 1.51, n_i= 0.0087 for the IRTM solar channel instrument). Modeling the wavelength-integrated values rather than integrating over the model *I/F* for each wavelength introduces a 5% error to the results, an acceptable increase in total error. The observations were taken on L_s 209, 212, 276, and 282, for which the optical depth of the dust was between 2 and 2.5 at the VL1 and VL2 sites. The difference in the model *I/F* with these high optical depths was less than 2%, so the upper limit was used for all observations. We used the specific observing geometry as an input for each model. We modeled each point and calculated the percent error for each point (i.e., $[(I/F_{obs} - I/F_m) / I/F_{obs}] \times 100$).

A simple multiple regression analysis was done in order to find the correlation between the percent difference of the observed-model Lambert albedos and the various observing parameters. The strongest correlations were with time (r = -0.4), incidence (r = -0.7), and phase (r = 0.5). The correlations are not high because the relationships are not strictly linear. Some of the greatest differences between our model and the observations occur in the late evening hours as well as early morning, thus the stronger correlation between incidence than time after sunrise. Furthermore, the majority of reflectance values of the observations are within 1 sigma and are modeled well, so the correlations are biased to 0. The correlations corroborate the earlier results for the VL1 site, that the brightest observations are anomalous points that are not strictly phase angle dependent.

3.2.2. Particle size. The second hypothesis assumes that the particles are a different size than that used paper 1. The particle size distributions that we investigate are those of *Drossart et al.* [1991] where r_{eff} = 1.24 μm and v_{eff} = 0.25 μm, our own model where r_{eff} = 1.85 μm and v_{eff} = 0.51 μm, and the *Toon et al.* [1977] model where r_{eff} = 2.5 μm and v_{eff} = 0.5 μm. In all of the cases tested the refractive indices of our wavelength-dependent model are used in order to separate the size effects. The particles are assumed to be nonspherical with nonspherical parameters described in paper 1, so that shape effects would be insignificant as well.

As would be expected in this sort of comparison in which the data are wavelength-integrated over the entire solar wavelength range, size effects are muted (Figure 4). The average difference in each case is small (2% for the Phobos model, 5% for the Viking model, and 7% for the Toon model). Although we can improve the results marginally by decreasing particle size, that is not enough to explain the model differences in the AM data.

3.2.3. Particle brightness. The third hypothesis assumes that the AM observations somehow include particles that are brighter than the model that we present. We consider for this comparison particles that are relatively bright (palagonite) and use the particle size distribution and shape from paper 1 in order to separate effects of the refractive indices.

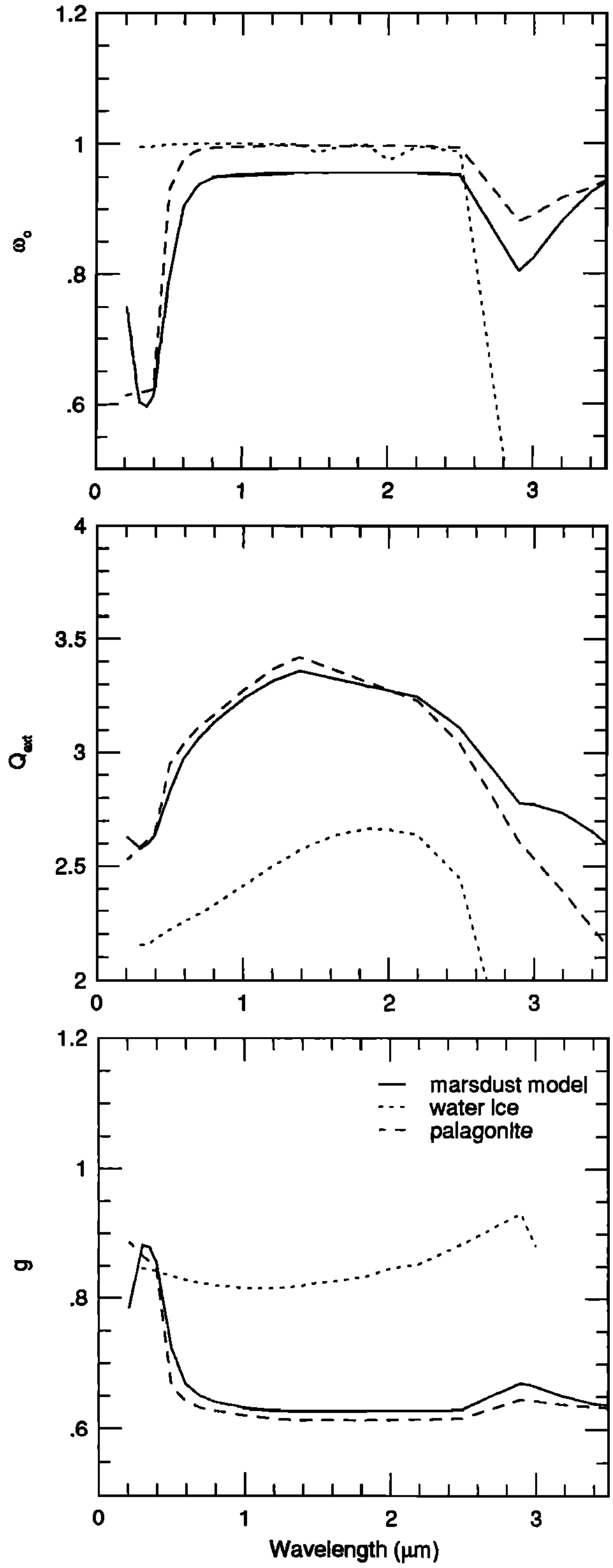

Figure 5. Comparison of the real and imaginary parts of the complex index of refraction for three substances: the marsdust model (solid line), water ice (dotted line), and a palagonite (dashed line).

Despite the wavelength integration, the solar channel data seem to be particularly sensitive to the absorbing qualities of the particles. The comparison of the scattering properties in Figure 5 demonstrates the absorbing qualities of three

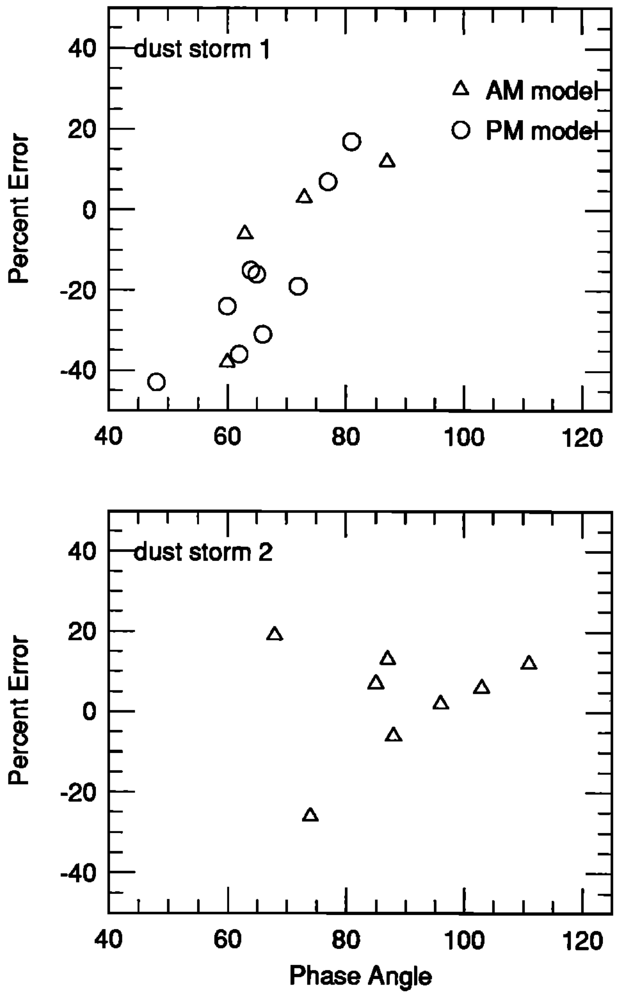

Figure 6. Comparison of the error in model results for the marsdust particle size distribution, shape and the complex index of refraction of the *Clark et al.* [1990] palagonite.

materials. Our marsdust model (the solid line) is the most absorbing. A palagonite (the dashed line [*Clark et al.*, 1990]) is slightly less absorbing but has the same basaltic features as our model (i.e., absorption peaks at 0.2 and 3.0 μm). Ice (the dotted line [*Warren*, 1984]) is much brighter in the ultraviolet and slightly more absorbing in the near-IR.

The models of the AM observations using our model (Figures 3 and 4b) indicate that the model dust particles are too absorbing. The model using palagonite particles provides insight as to whether the brighter particles of the same basaltic-type composition will better match the observations. Note that palagonite is a weathering product and that this specific palagonite is bright. Other weathering processes may produce darker palagonites. While there is some improvement in the model AM observations, the PM models are too bright (Figure 6). We assume that if the particles are brighter, that both AM and PM observations would be effected. That is, there is no reason to expect a diurnal variation in the composition. The afternoon observations are taken on the same L_S as the dust storm 1 AM observations, and so it is unlikely that mixing could darken the dust particles.

3.2.4. Particle composition. The fourth hypothesis is that ice particles form in the morning hours and evaporate in the afternoon hours. This hypothesis satisfies the requirement that AM particles be brighter than PM particles with simple meteorological phenomenon. In a detailed study of water condensation in the Martian atmosphere, *Colburn et al.* [1989] conclude that if water were to condense on dust particles the result would be water ice clouds in the upper atmosphere (above 12 km) and that the majority of the condensed water would evaporate by the afternoon.

In this study, we model ice cloud particles as a dust core surrounded by water ice. For computational convenience, the cloud particles are assumed to be spherical and stratified. A Mie scattering method is used to determine the scattering properties of such a combined particle [*Toon and Ackerman*, 1981]. The ice shell fraction chosen was 90% in order to obscure the effects of the darker dust particles. The ice shell fraction was added onto the dust particle, increasing the particle effective radius from 1.8 μm (no ice) to 3.5 μm (90% shell).

Michelangeli et al. [1993] model the microphysics of water ice clouds in the Martian atmosphere and conclude that the

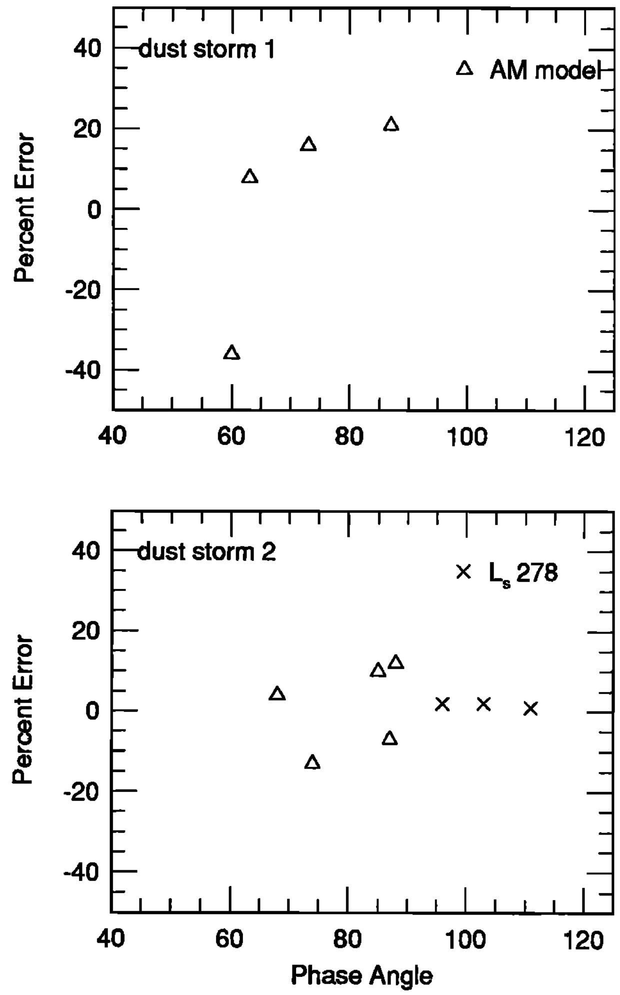

Figure 7. Comparison of the error in model results for dust particles encased in an ice shell. The particle size is increased by 90%, and the shape is spherical to simulate ice deposition on the marsdust particles. The real and imaginary indices of *Warren* [1984] are used to simulate the single-scattering properties of the water ice shell.

clouds are dynamic and need an exterior source of dust and water vapor to recur (i.e. clouds do not necessarily recur daily). Their simulations include dust with mean particle radii varying from 0.2 to 5.0 μm. According to their model, the dust/ice cloud particles can grow to 10 times their original size, during the course of a single cloud event. In our study the assumption of cloud particles with an ice shell of 90% and effective radius of 3 to 4 μm is not unreasonable. We do not include such effects as dynamically changing particle size distributions and the optical properties of mixtures of dust and ice particles.

In most cases there is a marked improvement in the model predictions for AM observations (Figure 7). Particularly for the observations in the early morning hours, up to 2 hours after sunrise, the model predictions are within 10% of the observed values. The most interesting set of observations occurs on L_s 278 in the early morning (the three points plotted with crosses in Figure 7). They are taken at fairly low phase and high optical depth, which are the optimum conditions for testing our marsdust model. Without the ice shell, the model predictions are an average of 30% darker than the observations. With the ice shell, the model results are within a few percent.

There is one observation during dust storm 1 that is anomalously dark (phase angle 60°). The best match to this observation is to increase the particle size to the Toon size distribution. Whether this is an example of the mixing that occurs during the dust storms or just an anomalous point is difficult to determine.

4. Summary

This paper attempts to define a new model for the Martian "atmospheric" dust, based on the work done by *Pollack et al.* [1995]. The single-scattering properties of the dust are modeled at all solar wavelengths (0.2 - 4.2 μm) using data taken by the Phobos-2 spacecraft and telescopic measurements. The bright Martian soil is assumed to be an analog for the Martian dust. The complex index of refraction is extracted using Hapke theory, based on the analysis of the Martian surface at the VL1 site done by *Arvidson et al.* [1989] and the analysis of the Martian airborne dust done by *Pollack et al.* [1995].

The results of this process are the "marsdust" model (Figure 2 and Table 2). The single-scattering properties vary from previous observations and models, but not significantly. The model shows optical behavior indicative of a basaltic compound; however, any detailed information about the mineral composition is lost in the retrieval algorithm. As with most basalts, there is a strong spectral variation of the imaginary index of refraction over the entire solar wavelength range.

By modeling data taken by the Viking Orbiter IRTM solar channel, we find that the new marsdust model is a good representation for the atmospheric dust in the solar wavelengths. Changes of 10% or more in effective particle size do not largely change the model results, since the data are wavelength-integrated over the solar spectrum. The marsdust model does not match some morning observations well. This is most likely due to changes in composition. The brightest morning observations can be modeled by including an ice shell around the dust particles, such as would occur with the formation of ice clouds. Thus, the particles become brighter in the morning hours, when ice deposition is most likely to occur. This improves the models of the observations by as much as 40%. Other hypotheses, such as vertical mixing of brighter minerals and smaller or larger particles sizes, do not model the morning observations well.

Acknowledgments. The authors thank B. Haberle, J Murphy, J. Schaeffer, D. Crisp, J. Cuzzi, and a host of other scientists for their encouragement to finish this project and for their helpful suggestions after the death of Jim Pollack. Conversations with Dave Crisp about similar research done in *Santee and Crisp* (1993) were inspiring. Many thanks for his help. We thank P. Gierasch and C. Sagan for their support while the final version of this manuscript was completed. The reviews by M. Wolff and M. Mellon were essential in the completion of this manuscript and greatly appreciated This research was carried out at NASA Ames Research Center and San Jose State University under research contract JRI NA2-740 and JRI NCC2-5708. This work was supported in part by a grant from NASA's Planetary Atmospheres program, RTOP 154-10-80-01.

References

Allen, C. W., Astrophysical Quantities, Athlone, London, 1985.

Arvidson, R. E., E. A. Guinness, M A. Dale-Bannister, J. Adams, M. Smith, P. R. Christensen, and R. B. Singer, Nature and distribution of surficial deposits in Chryse Planitia and vicinity, Mars, *J. Geophys Res., 94,* 1573-1587, 1989.

Bell, J.F., III, T.B. McCord, and P.D. Owensby, Observational evidence of crystalline iron oxides on Mars, *J. Geophys. Res., 95,* 14,447-14,461, 1990.

Bibring, J.-P, *et al.*, Results from the ISM experiment, *Nature, 341,* 591-592, 1989.

Chase, S. C., J. L. Engel, H. W. Eyerly, H. H. Kieffer, F. D. Palluconi, and D Schofield, Viking infrared thermal mapper, *Appl. Opt., 17,* 1243-1251, 1978

Chylek, P , and G. W. Grams, Scattering by nonspherical particles and optical properties of Martian dust, *Icarus, 36,* 198-203, 1978.

Clancy, R.T., S.W. Lee, G. R. Gladstone, W. McMillan, and T. Roush, A new model for Mars atmospheric dust based upon analysis of ultraviolet through infrared observations from Mariner 9, Viking, and Phobos, *J. Geophys. Res., 100,* 5251-5263, 1995

Clark, R. N., G. A. Swayze, R. B. Singer, and J. B. Pollack, High-resolution reflectance spectra of Mars in the 2 3 μm region: Evidence for the mineral scapolite, *J. Geophys Res., 95,* 14,463-14,480, 1990.

Colburn, D. J., J. B. Pollack, and R. Haberle, Diurnal variations in optical depth at Mars, *Icarus, 79,* 159-189, 1989.

Domingue, D. L., B. W. Hapke, G. W. Lockwood, and D T. Thompson, Europa's phase curve: Implications for surface structure, *Icarus, 90,* 30-42, 1991.

Drossart, P., J. Rosenqvist, S Erard, Y. Langevin, J.-P. Bibring and M. Combes, Martian aerosol properties from the Phobos ISM experiment, *Ann. Geophys., 9,* 754-760, 1991.

Egan, W. G., T. Hilgeman, and L. L. Smith, Comparison between infrared martian disk spectra and optical properties of terrestrial analogues, *Icarus, 35,* 209-226, 1978

Hansen, J.E., Radiative transfer by doubling very thin layers, *Astrophys. J., 155,* 565, 1969.

Hapke, B., Bidirectional reflectance spectroscopy, 1, Theory, *J. Geophys Res., 86,* 3039-3054, 1981.

Hapke, B., Bidirectional reflectance spectroscopy, 4, The extinction coefficient and the opposition effect, *Icarus, 67,* 264-280, 1986

Houck, J.R., J.B. Pollack, C. Sagan, D Schaack, and J. Decker, High altitude infrared spectroscopic evidence for bound water on Mars, *Icarus, 18,* 470-480, 1973.

Kahn, R. A , T Z. Martin, R. W. Zurek, and S. W. Lee, The Martian dust cycle, in *Mars*, edited by H. H. Kieffer, B M Jakosky, C. W. Snyder, and M. S. Matthews, p. 1017, Univ. of Arizona Press, Tucson, 1992.

Kieffer, H. H., T. Z. Martin, A. R. Peterfreund, and B. M. Jakosky, Thermal and albedo mapping of Mars during the Viking primary mission, *J. Geophys. Res., 82,* 4249-4291, 1977.

Korablev, O. I., V. A. Krasnopolsky, A. V. Rodin, and E. Chassefiere, Vertical structure of Martian dust measured by solar infrared occultations from the Phobos spacecraft, *Icarus, 102,* 76-87, 1993.

Martin, T. Z., Thermal infrared opacity of the Mars atmosphere, *Icarus, 66,* 2-21, 1986.

McCord, T. B., R. L. Huguenin, D. Mink, and C. Pieters, Spectral reflectance of Martian areas during the 1973 opposition: Photoelectric filter photometry 0.33 - 1.10 µm, *Icarus, 31,* 25-39, 1977.

Michelangeli, D. V., O. B. Toon, R. M. Haberle and J. B. Pollack, Numerical simulations of the formation and evolution of water ice clouds in the martian atmosphere, *Icarus, 100,* 261-285, 1993.

Mustard, J F., and J.F. Bell III, New composite reflectance spectra of Mars from 0.4 to 3.14 µm, *Geophys. Res. Lett., 21,* 353-356, 1994.

Mustard, J.F., S. Erard, J.-P. Bibring, J.W. Head, S. Hurtrez, Y. Langevin, C.M. Pieters, and C.J. Sotin, The surface of Syrtis Major: Composition of the volcanic substrate and mixing with altered dust and soil, *J. Geophys. Res., 98,* 3387-3400, 1993.

Owen, T., and C. Sagan, Minor constituents in planetary atmospheres: Ultraviolet spectroscopy from the Orbiting Astronomical Observatory, *Icarus, 16,* 557-568, 1972.

Pang, K., J. M. Ajello, C. W. Hord, and W. G. Egan, Complex refractive index of Martian dust: Mariner 9 ultraviolet observations, *Icarus, 27,* 55-67, 1976.

Pollack, J. B., and J N. Cuzzi, Scattering by nonspherical particles of size comparable to a wavelength: A new semi-empirical theory and its application to tropospheric aerosols, *J. Atmos. Sci., 37,* 868-881, 1980.

Pollack, J. B., D. S. Colburn, F. M. Flaser, R. Kahn, C. E. Carlson, and D. C. Pidek, Properties and effects of dust suspended in the Martian atmosphere, *J. Geophys. Res., 84,* 2929-2945, 1979.

Pollack, J B., O. B. Toon, and B. N. Khare, Optical properties of some terrestrial rocks and glasses, *Icarus, 19,* 372-389, 1973.

Pollack, J. B., M. E. Ockert-Bell, and M. K. Shepard, Viking Lander image analysis of Martian atmospheric dust, *J. Geophys. Res., 100,* 5235-5250, 1995.

Roush, T. L., E. A. Roush, R. B. Singer, and P. G. Lucey, Estimates of absolute flux and radiance factor of localized regions on Mars in the 2-4 µm wavelength region, *Icarus, 99,* 42-50, 1992.

Santee, M., and D. Crisp, Thermal structure and dust loading of the Martian atmosphere during late southern summer: Mariner 9 revisited, *J. Geophys. Res., 98,* 3261-3279, 1993.

Toon, O. B., and T. Ackermann, Algorithms for the calculation of scattering by stratified spheres, *Appl. Opt., 20,* 3657-3660, 1981.

Toon, O. B., J. B. Pollack, and C. Sagan, Physical properties of particles composing the Martian dust storm of 1971-1972, *Icarus, 30,* 663-696, 1977.

van de Hulst, H. C., *Light Scattering by Small Particles,* Dover, New York, 1981.

Wallace, L., J.J. Caldwell and B.D. Savage, Ultraviolet photometry from the Orbiting Astronomical Observatory, III, Observations of Venus, Mars, Jupiter, and Saturn longward of 2000 Å, *Astrophys. J., 172,* 755, 1972.

Warren, S. G., Optical constants of ice from the ultraviolet to the microwave, *Appl. Opt., 23,* 1206-1225, 1984.

Wolff, M. J., S. W. Lee, R. T. Clancy, L. Martin, J. F. Bell III, and P. James, 1995 observations of Martian dust storms using the Hubble space telescope, *J. Geophys. Res., 102,* 1679-1692.

J F. Bell III and M. E. Ockert-Bell, Center for Radiophysics and Space Research, Cornell University, 324 Space Sciences Building, Ithaca, NY 14853-6801. (email: jimbo@marswatch.tn.cornell.edu, mbell@astrosun.tn.cornell.edu)

F. Forget, Laboratoire de Meteorologie Dynamique du CNRS, 24 rue Lhomonde, 75231 Paris Cedex 05, France. (email: forget@lmd.ens.fr)

C P. McKay, Space Sciences Division, NASA Ames Research Center MS 245-3, Moffett Field, CA 94035. (email: mckay@gal.arc.nasa.gov)

(Received June 7, 1996, revised December 12, 1996; accepted December 19, 1996.)